# High order methods in CFD
## Discontinuous Galerkin Method

Praveen Chandrashekar

praveen@math.tifrbng.res.in

http://cpraveen.github.io

Center for Applicable Mathematics
Tata Institute of Fundamental Research
Bangalore-560065, India
http://math.tifrbng.res.in

CEP Lecture, DRDL, Hyderabad
16 October 2019

# Finite element Galerkin Method

$$\partial_t \boldsymbol{U} + \boldsymbol{R}(\boldsymbol{U}) = 0$$

1. approximate solution in terms of some basis/trial functions

$$\boldsymbol{U}(x,t) \approx \boldsymbol{U}_h(x,t) = \sum_j \boldsymbol{U}_j \phi_j(x)$$

2. satisfy PDE in a weak manner: make residual orthogonal to all test functions=trial functions

$$\int_\Omega [\partial_t \boldsymbol{U}_h + \boldsymbol{R}(\boldsymbol{U}_h)] \phi_i(x) \mathrm{d}x = 0, \qquad \forall \phi_i$$

$\phi_i$ discontinuous $\implies$ discontinuous Galerkin method

# DG for hyperbolic problems

## DG in 1-D

Conservation law in 1-D

$$\boldsymbol{U}_t + \boldsymbol{F}(\boldsymbol{U})_x = 0, \qquad x \in [a,b], \quad t > 0$$

Partition domain $[a,b]$ into disjoint elements
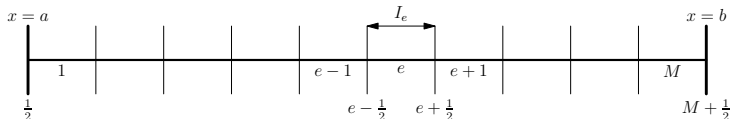


$$I_e = [x_{e-\frac{1}{2}}, x_{e+\frac{1}{2}}], \qquad h_e = x_{e+\frac{1}{2}} - x_{e-\frac{1}{2}}, \qquad [a,b] = \cup_e I_e$$

Inside each element, approximate solution by polynomial of degree $N \geq 0$

$$x \in I_e: \qquad \boldsymbol{U}_h(x,t) = \boldsymbol{U}^e(x,t) = \sum_{i=0}^{N} \boldsymbol{U}_i^e(t)\phi_i^e(x) \in \mathbb{P}_N(x)$$

$\{\phi_0^e, \phi_1^e, \ldots, \phi_N^e\}$ is a basis for $\mathbb{P}_N$.

# DG in 1-D

The solution $\boldsymbol{U}_h$ is allowed to be discontinuous at the element boundaries.



i.e.,

$$\boldsymbol{U}^e(x_{e+\frac{1}{2}}) \neq \boldsymbol{U}^{e+1}(x_{e+\frac{1}{2}})$$

# DG in 1-D
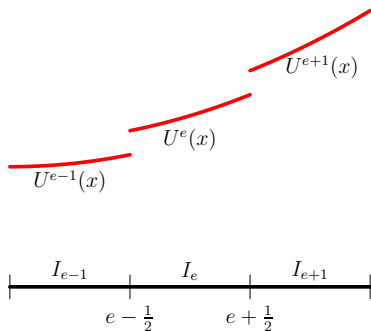
Galerkin method

$$\int_{I_e} [\boldsymbol{U}_t + \boldsymbol{F}(\boldsymbol{U})_x] \, \phi_i^e \mathrm{d}x = 0$$

Perform integration by parts: $i = 0, 1, \ldots, N$

$$\frac{\mathrm{d}}{\mathrm{d}t} \int_{I_e} \boldsymbol{U}^e \phi_i^e \mathrm{d}x - \int_{I_e} \boldsymbol{F}(\boldsymbol{U}^e) \frac{\partial \phi_i^e}{\partial x} \mathrm{d}x + (\boldsymbol{F}\phi_i^e)_{x=x_{e+\frac{1}{2}}} - (\boldsymbol{F}\phi_i^e)_{x=x_{e-\frac{1}{2}}} = 0$$

Approximate flux at $x = x_{e+\frac{1}{2}}$ by a numerical flux function $\hat{\boldsymbol{F}}$

$$\boldsymbol{F}(x_{e+\frac{1}{2}}, t) \approx \boldsymbol{F}_{e+\frac{1}{2}}(t) = \hat{\boldsymbol{F}}(\boldsymbol{U}^e(x_{e+\frac{1}{2}}, t), \boldsymbol{U}^{e+1}(x_{e+\frac{1}{2}}, t))$$

First term is

$$\int_{I_e} \boldsymbol{U}^e \phi_i^e \mathrm{d}x = \int_{I_e} \sum_{j=0}^{N} \boldsymbol{U}_j^e \phi_j^e \phi_i^e \mathrm{d}x = \sum_{j=0}^{N} M_{ij}^e \boldsymbol{U}_j^e$$

## DG in 1-D

Mass matrix $M^e \in \mathbb{R}^{(N+1) \times (N+1)}$

$$M_{ij}^e = \int_{I_e} \phi_i^e \phi_j^e \mathrm{d}x$$

System of ODE

$$M^e \frac{\mathrm{d}U^e}{\mathrm{d}t} + R^e(U^{e-1}, U^e, U^{e+1}) = 0$$

where for $i = 0, 1, \ldots, N$

$$R_i^e = - \int_{I_e} \boldsymbol{F}(\boldsymbol{U}^e) \frac{\partial \phi_i^e}{\partial x} \mathrm{d}x + \boldsymbol{F}_{e+\frac{1}{2}} \phi_i^e(x_{e+\frac{1}{2}}) - \boldsymbol{F}_{e-\frac{1}{2}} \phi_i^e(x_{e-\frac{1}{2}})$$

Integrate ODE using SSPRK schemes [45]
Popularized in a series of papers by Cockburn & Shu [17], [16], [15], [19]

# Some remarks

1. Method is conservative
2. Numerical fluxes are same as those used in finite volume methods
   - upwind/Riemann solver based fluxes must be used
3. Smooth solutions
$$\|\boldsymbol{U} - \boldsymbol{U}_h\| = O(h^{N+1})$$
4. Each element is coupled to its left and right neighbor only, via numerical flux
5. Same stencil $\{e - 1, e, e + 1\}$ for all order of accuracy
6. Evolve entire polynomial solution, not just cell average
   - No solution reconstruction required
7. High order upto the boundary
   - no need to change scheme near boundary
8. Low dissipation and dispersion errors
9. Fixed, compact stencil, high arithmetic intensity: good for HPC

## Implementation details: mapped elements, modal basis

Define basis functions on a reference element, e.g., $[-1, 1]$

$$I_e \to [-1, 1], \qquad \xi = \frac{x - x_e}{\frac{1}{2}h_e} \in [-1, 1]$$

Modal basis: basis of orthogonal polynomials

$$P_i = \text{Legendre polynomial of degree } i$$

$$\phi_i^e(x) = \phi_i(\xi) = \sqrt{2i+1}P_i(\xi)$$

Mass matrix is diagonal

$$M^e = h_e \mathbb{I}_{N+1}, \qquad \mathbb{I}_{N+1} = (N+1) \times (N+1) \text{ identity matrix}$$

Example: degree $N = 1$

$$\boldsymbol{U}_h^e = \boldsymbol{U}_0^e + \boldsymbol{U}_1^e \xi = \boldsymbol{U}_0^e + \boldsymbol{U}_1^e \frac{x - x_e}{\frac{1}{2}h_e}$$

$$\boldsymbol{U}_0^e = \text{cell average}, \qquad \boldsymbol{U}_1^e = \text{undivided slope}$$

## Implementation details: mapped elements, nodal basis

Choose $N+1$ distinct points in reference element $[-1,1]$

$$-1 \leq \xi_0 < \xi_1 < \ldots < \xi_N \leq +1$$

Basis functions are Lagrange polynomials
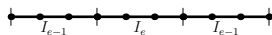
$$\phi_i^e(x) = \ell_i(\xi) = \prod_{j=0, j \neq i}^{N} \frac{\xi - \xi_j}{\xi_i - \xi_j}, \qquad \ell_i(\xi_j) = \delta_{ij} = \begin{cases} 1 & i = j \\ 0 & \text{otherwise} \end{cases}$$

Coefficients are nodal solution values

$$\boldsymbol{U}^e(\xi) = \sum_{j=0}^{N} \boldsymbol{U}_j^e \ell_j(\xi), \qquad \boldsymbol{U}_j^e = \boldsymbol{U}^e(\xi_j)$$

Nodes are usually taken to be Gauss-Legendre or Gauss-Lobatto-Legendre quadrature points

# Implementation details: quadrature

- Integrals: need numerical quadrature due to non-linear flux functions
- Optimal accuracy: quadrature rule for flux integral must be exact for polynomials of degree atleast $2N$.
- Gauss-Legendre or Gauss-Legendre-Lobatto quadrature use $Q = N + 1$ point rule
- Mass matrix can also be computed by quadrature
- Nodal basis of GL nodes; use same nodes for quadrature
  - ▶ mass matrix is exact (1-D)
  - ▶ mass matrix is diagonal
- Nodal basis of GLL nodes; use same nodes for quadrature
  - ▶ mass matrix is not exact
  - ▶ mass matrix is diagonal

# Example: linear advection
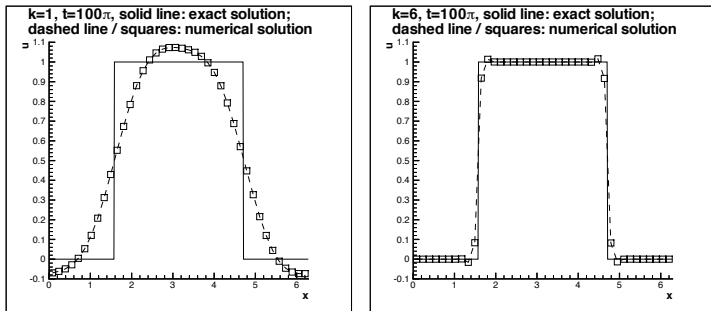


Fig. 2.1. *The discontinuous Galerkin method (2.4) applied to the linear equation (2.1) with a square initial condition, $t = 100\pi$. 40 cells. Third order Runge-Kutta in time. Solid line: the exact solution; Dashed line and squares symbols: the computed solution at the cell centers. Left: $k = 1$; Right: $k = 6$.*

# DG for parabolic problems

# DG for heat equation: $u_t = u_{xx}$

$$\int_{I_e} \phi_i^e \partial_t u_h \mathrm{d}x + \int_{I_e} (\partial_x u_h)(\partial_x \phi_i^e)\mathrm{d}x + (\phi_i^e \partial_x u_h)_{e-\frac{1}{2}} - (\phi_i^e \partial_x u_h)_{e+\frac{1}{2}} = 0$$

Question: How to approximate heat flux $(\partial_x u_h)_{e+\frac{1}{2}}$ ?

$$(\partial_x u_h)_{e+\frac{1}{2}} = \frac{1}{2}[(\partial_x u_h)_{e+\frac{1}{2}}^- + (\partial_x u_h)_{e+\frac{1}{2}}^+]$$
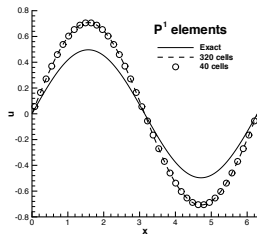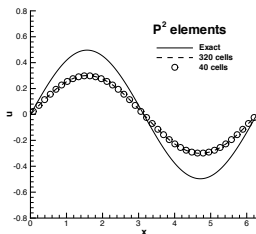


Converges to wrong solution !!!

Fig. 2.1. The numerically inconsistent discontinuous Galerkin method (2.8) applied to the heat equation (2.1) with an initial condition $u(x,0) = \sin(x)$. $t = 0.7$. Third-order Runge–Kutta in time with small $\Delta t$ so that time error can be ignored. Numerical solutions with 40 cells (circles) and 320 cells (dashed lines), vs. the exact solution (solid line). (a) $k = 1$; (b) $k = 2$.

Zhang & Shu [48]

# DG for parabolic problems

Two methods for stable and accurate schemes
- Interior penalty methods
  - ▶ Primal method, no extra variables
  - ▶ Add extra terms to get stability: symmetric and non-symmetric IP
  - ▶ Elliptic/parabolic: Douglas/Dupont [23], Arnold [2]
  - ▶ Navier-Stokes: Hartmann [34], Chandrashekar [10][1]
- Mixed methods
  - ▶ Write as first order system

  $$u_t = q_x, \qquad q = u_x$$

  Apply DG scheme to this system
  - ▶ Both $u$ and $q$ can be computed accurately
- Unified analysis presented in [3]

---
[1]Based on KFVS: see my slides

# DG for parabolic problems: mixed methods

$$u_t = q_x, \qquad q = u_x$$

Approximate both $u$ and $q$ using piecewise polynomials

$$u \approx u_h \in \mathbb{P}_N, \qquad q \approx q_h \in \mathbb{P}_N$$

Integrate by parts on one element

$$\int_{I_e} \phi_i^e \frac{\partial u_h}{\partial t} \mathrm{d}x + \int_{I_e} q_h \frac{\partial \phi_i^e}{\partial x} \mathrm{d}x + \phi_i^e(x_{e-\frac{1}{2}}^+) q_{e-\frac{1}{2}} - \phi_i^e(x_{e+\frac{1}{2}}^-) q_{e+\frac{1}{2}} = 0$$

$$\int_{I_e} \phi_i^e q_h \mathrm{d}x + \int_{I_e} u_h \frac{\partial \phi_i^e}{\partial x} \mathrm{d}x + \phi_i^e(x_{e-\frac{1}{2}}^+) u_{e-\frac{1}{2}} - \phi_i^e(x_{e+\frac{1}{2}}^-) u_{e+\frac{1}{2}} = 0$$

Require numerical fluxes: $u_{e+\frac{1}{2}}$, $q_{e+\frac{1}{2}}$

## DG for parabolic problems: Numerical fluxes

**BR1 scheme** (Bassi & Rebay [5])

$$u_{e+\frac{1}{2}} = \frac{1}{2}(u^-_{e+\frac{1}{2}} + u^+_{e+\frac{1}{2}}), \qquad q_{e+\frac{1}{2}} = \frac{1}{2}(q^-_{e+\frac{1}{2}} + q^+_{e+\frac{1}{2}})$$

- Sub-optimal error: $\|u - u_h\| = O(h^N)$
- Large stencil: neighbour of neighbour
- Odd-even decoupling

**BR2 scheme** [9]
- local lifting operator to define face-based flux
- compact stencil: face neigbours only
- optimal order accuracy for all degree

# DG for parabolic problems: Numerical fluxes

**LDG scheme**: alternating flux (Cockburn & Shu [18])

$$u_{e+\frac{1}{2}} = u^-_{e+\frac{1}{2}}, \qquad q_{e+\frac{1}{2}} = q^+_{e+\frac{1}{2}}$$
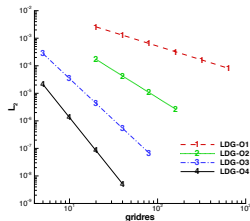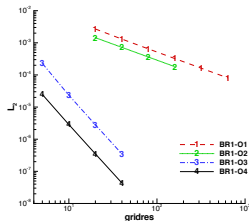
- Optimal accuracy: $\|u - u_h\| = O(h^{N+1})$ for all $N$
- Smaller stencil

**CDG scheme**: (Persson & Peraire [43])
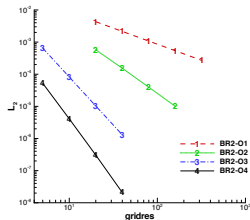


(Landmann [39])

# Fourier analysis

# Dissipation & dispersion property

For more details, see my DG notes

$$U_h^e(x, t) = \hat{U} \exp(i(kx_e - \omega t)) \quad \implies \quad A(kh)\hat{U} = -i\omega h \hat{U}$$

Ideal dispersion relation: $\omega = k$, no dissipation, no dispersion.
Numerical dispersion relation:
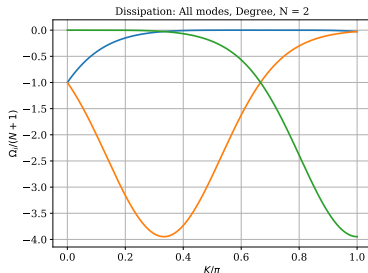
$$Imag(\omega) : \text{dissipation} \qquad Real(\omega) : \text{dispersion}$$
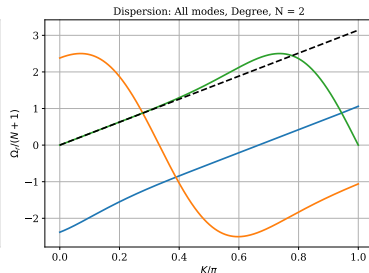


Degree $N = 2$, physical mode is in green

# Dissipation & dispersion property
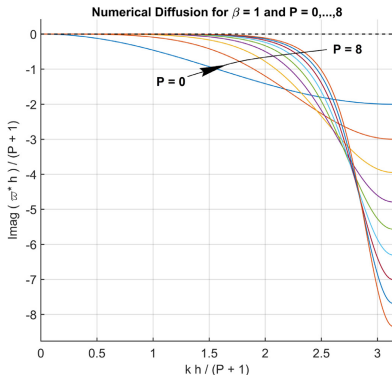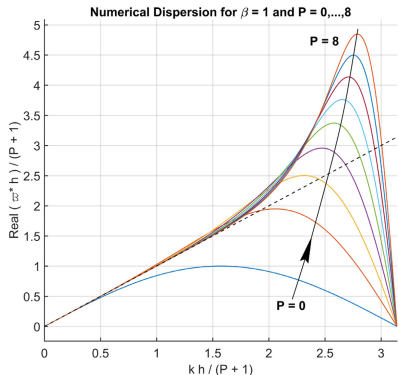


Mengaldo et al. [41]

# Dissipation & dispersion property

Dispersion: $\qquad |Re(\tilde{\omega}^*) - \tilde{k}| < 0.01$

Maximum resolved wave number and minimum number of unknowns per wavelength for DG schemes, central FD schemes and the DRP scheme.

| Scheme | Wave number | Unknowns per wavelength |
|---|---|---|
| DG-$P^1$ | 0.7716 | 8.1430 |
| DG-$P^2$ | 0.9942 | 6.3193 |
| DG-$P^3$ | 1.1567 | 5.4318 |
| DG-$P^4$ | 1.2754 | 4.9266 |
| DG-$P^5$ | 1.3653 | 4.6020 |
| FD 2nd order | 0.3925 | 16.0075 |
| FD 4th order | 0.7980 | 7.8733 |
| FD 6th order | 1.0841 | 5.7955 |
| optimized 7-point DRP | 1.2469 | 5.0390 |

(Cheng & Shu [14])

# Dissipation & dispersion property
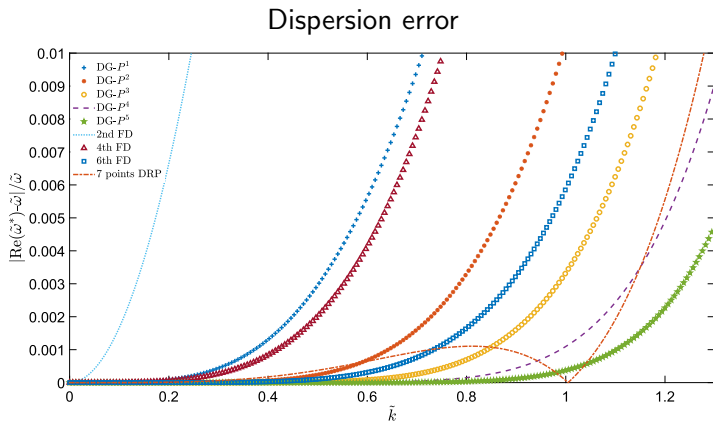


Dispersion error

**Fig. 3.3.** Relative errors of Re($\tilde{\omega}$) for DG schemes and central FD schemes.

(Cheng & Shu [14])

# Dissipation & dispersion property
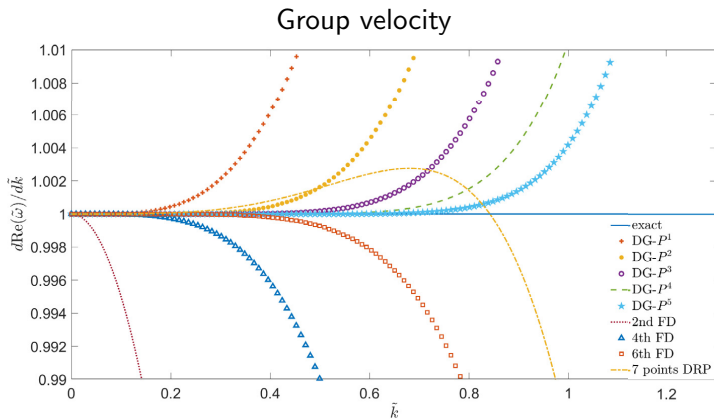
(Cheng & Shu [14])

# Dissipation & dispersion property

## Linear advection: Comprison of FD vs DG
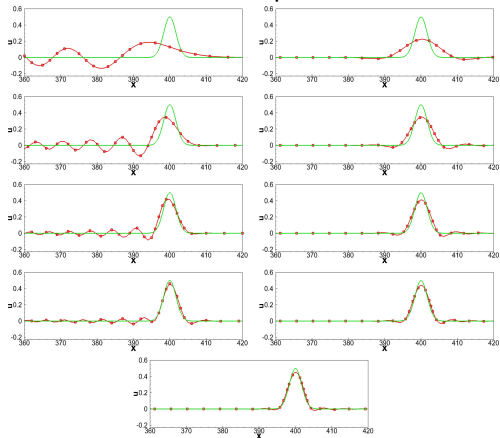


**Fig. 6.1.** Comparisons between the numerical and exact solutions of the convective wave equation. $b = 2$, $t = 400$, $h_{FD} = 1$, $h_{DG-P^k} = q + 1$. Lines without square symbols correspond to exact solutions while lines with square symbols correspond to numerical solutions. The subgraphs from top to bottom on the left correspond to FD schemes of order 2, 4, 6, optimized 7-point DRP scheme, and the subgraphs from top to bottom on the right correspond to DG $P^1 - P^4$. The bottom subgraph corresponds to DG-$P^5$.

(Cheng & Shu [14])

# Dissipation & dispersion property

- Comparison with compact schemes [1]
- One physical mode, several non-physical/parasitic modes
- Physical mode determines dominant behaviour at low wave-numbers
- All modes contribute to solution behaviour at large wave-numbers
  - ▶ Non-modal analysis [25]
  - ▶ Combined mode analysis [1]

# DG in multiple dimensions

# Types of basis functions

$\mathbb{P}_N$: complete polynomials

- Example: $\mathbb{P}_1 = \text{span}\{1, x, y\}$
- Used on triangles/tetrahedra
- Nodal Lagrange (many options) or modal (Jacobi polynomials)

$\mathbb{Q}_N$: tensor product polynomials

- Example: $\mathbb{Q}_1 = \text{span}\{1, x, y, xy\}$
- Used on quadrilateral/hexahedra
- Nodal Lagrange (GL or GLL) or modal (tensor product of Legendre)

Basis functions defined on mapped elements

Basis functions defined on real elements: Taylor basis [40]

# Mappings

Map element $K$ to reference element $\hat{K}$

$$\boldsymbol{x} \in K, \qquad \boldsymbol{\xi} \in \hat{K}$$

$$F_K : \hat{K} \to K$$

$$\boldsymbol{x} = F_K(\boldsymbol{\xi})$$

E.g., $\hat{K} = [0,1] \times [0,1]$ if $K$ is a quadrilateral
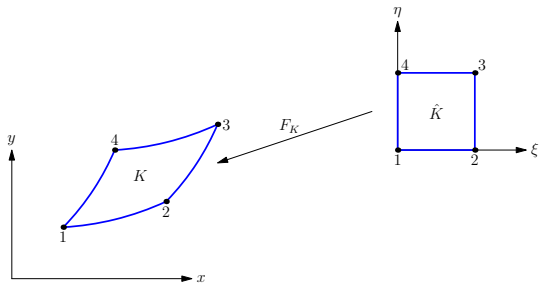


- $K$ triangle/tetrahedron: $F_K$ is an affine map
- $K$ quadrilateral/hexahedra: $F_K$ is bi/tri-linear map
- $K$ can be curved element: $F_K$ given in terms of Lagrange polynomials of degree $M \geq 1$

$$\boldsymbol{x} = \sum_{i=0}^{M} \sum_{j=0}^{M} \boldsymbol{x}_{ij} \ell_i(\xi) \ell_j(\eta)$$
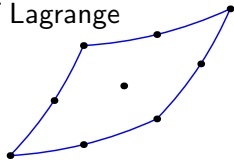
# DG for 2-D NS

$$\partial_t \boldsymbol{U} + \nabla \cdot \boldsymbol{F}(\boldsymbol{U}) = \nabla \cdot \boldsymbol{G}(\boldsymbol{U}, \nabla \boldsymbol{U})$$

Write as first order system

$$\partial_t \boldsymbol{U} + \nabla \cdot \boldsymbol{F}(\boldsymbol{U}) = \nabla \cdot \boldsymbol{G}(\boldsymbol{U}, \boldsymbol{Q}), \qquad \boldsymbol{Q} = \nabla \boldsymbol{U}$$

Inside each element $K$, approximate by degree $N$ polynomials

$$\boldsymbol{U}_h = \sum_{i=0}^{N} \sum_{j=0}^{N} \boldsymbol{U}_{ij}^K \phi_i(\xi) \phi_j(\eta), \qquad \boldsymbol{Q}_h = \sum_{i=0}^{N} \sum_{j=0}^{N} \boldsymbol{Q}_{ij}^K \phi_i(\xi) \phi_j(\eta)$$
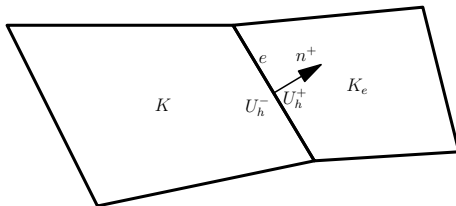
# DG for 2-D NS

Multiply by test function $\Phi_h$ and integrate on element $K$

$$\int_K (\Phi_h \partial_t \boldsymbol{U}_h - \boldsymbol{F}(\boldsymbol{U}_h) \cdot \nabla \Phi_h + \boldsymbol{G}(\boldsymbol{U}_h, \boldsymbol{Q}_h) \cdot \nabla \Phi_h) \mathrm{d}\boldsymbol{x}$$

$$+ \sum_{e \in \partial K_i} \int_e \Phi_h^- [\boldsymbol{F}(\boldsymbol{U}_h^-, \boldsymbol{U}_h^+, \boldsymbol{n}^+) - \boldsymbol{G}(\boldsymbol{U}_h^-, \boldsymbol{Q}_h^-, \boldsymbol{U}_h^+, \boldsymbol{Q}_h^+, \boldsymbol{n}^+)] \mathrm{d}s$$

$$+ \sum_{e \in \partial K_b} \int_e \Phi_h [\boldsymbol{F}(\boldsymbol{U}_h, \boldsymbol{U}_b, \boldsymbol{n}) - \boldsymbol{G}(\boldsymbol{U}_h, \boldsymbol{Q}_h, \boldsymbol{U}_b, \boldsymbol{Q}_b, \boldsymbol{n})] \mathrm{d}s = 0$$

$$\int_K (\Phi_h \boldsymbol{Q}_h + \boldsymbol{U}_h \nabla \Phi_h) \mathrm{d}\boldsymbol{x} - \sum_{e \in \partial K_i} \int_e \boldsymbol{U}(\boldsymbol{U}_h^-, \boldsymbol{U}_h^+) \Phi_h^- \boldsymbol{n}^+ \mathrm{d}s$$

$$- \sum_{e \in \partial K_b} \int_e \boldsymbol{U}_b \Phi_h \boldsymbol{n} \mathrm{d}s = 0$$

Each $\Phi_h$ is of the form $\phi_i(\xi)\phi_j(\eta), 0 \le i, j \le N$

## DG for 2-D NS

$\boldsymbol{F}(\boldsymbol{U}_h^-, \boldsymbol{U}_h^+, \boldsymbol{n}^+)$: inviscid numerical flux

**BR1 scheme**

$$\begin{aligned}
\boldsymbol{U}(\boldsymbol{U}_h^-, \boldsymbol{U}_h^+) &= \frac{1}{2}(\boldsymbol{U}_h^- + \boldsymbol{U}_h^+) \\
\boldsymbol{G}(\boldsymbol{U}_h^-, \boldsymbol{Q}_h^-, \boldsymbol{U}_h^+, \boldsymbol{Q}_h^+, \boldsymbol{n}^+) &= \frac{1}{2}[\boldsymbol{G}(\boldsymbol{U}_h^-, \boldsymbol{Q}_h^-, \boldsymbol{n}^+) + \boldsymbol{G}(\boldsymbol{U}_h^+, \boldsymbol{Q}_h^+, \boldsymbol{n}^+)]
\end{aligned}$$

Gassner et al. [30] show stability of this scheme for GLL nodes.

**LDG scheme**

$$\begin{aligned}
\boldsymbol{U}(\boldsymbol{U}_h^-, \boldsymbol{U}_h^+) &= \boldsymbol{U}_h^- \\
\boldsymbol{G}(\boldsymbol{U}_h^-, \boldsymbol{Q}_h^-, \boldsymbol{U}_h^+, \boldsymbol{Q}_h^+, \boldsymbol{n}^+) &= \boldsymbol{G}(\boldsymbol{U}_h^+, \boldsymbol{Q}_h^+, \boldsymbol{n}^+)
\end{aligned}$$

**Time stepping**: Explicit RK or implicit schemes

# Inviscid isentropic vortex
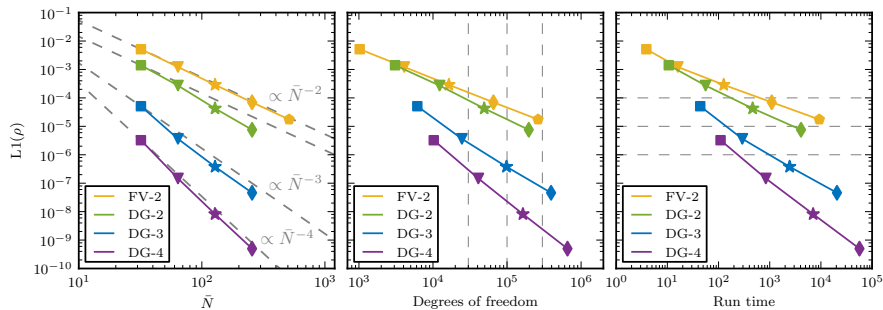


(Schaal et al. [44])
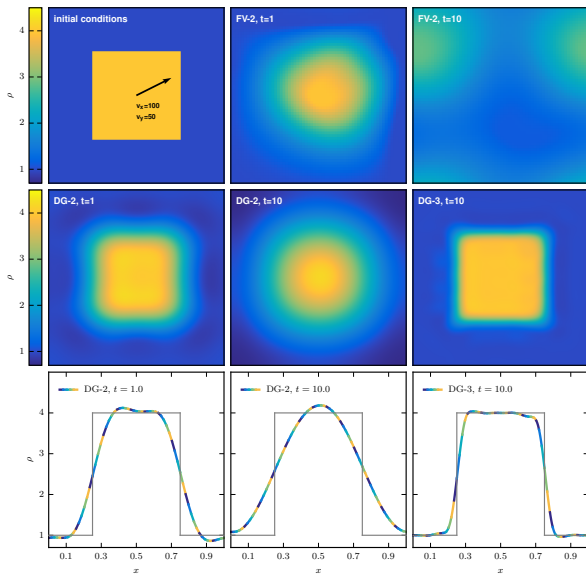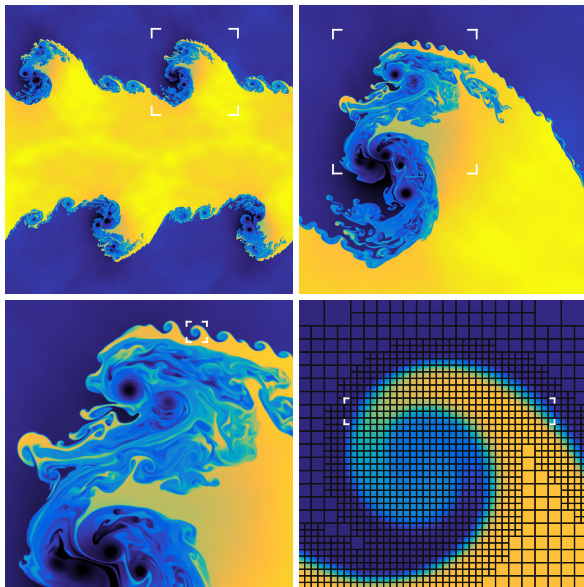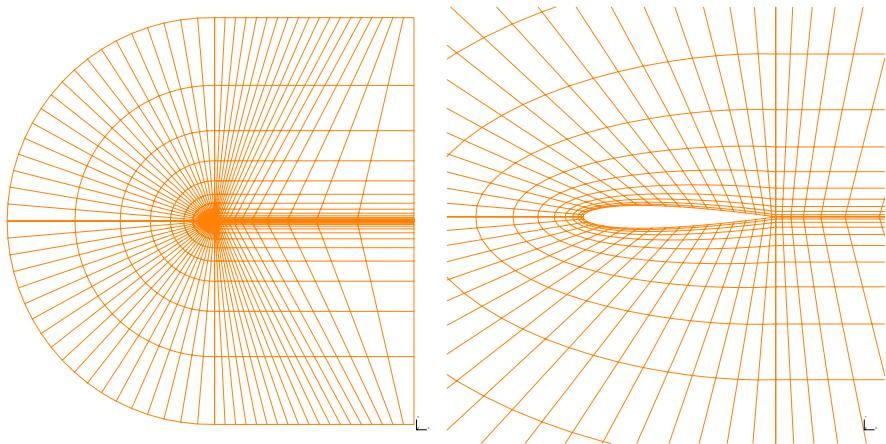
# Boundary approximation



True boundary

Isoparametric element
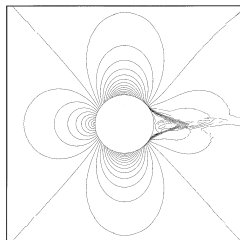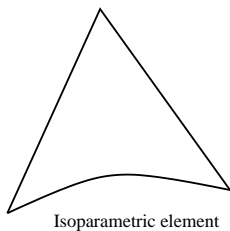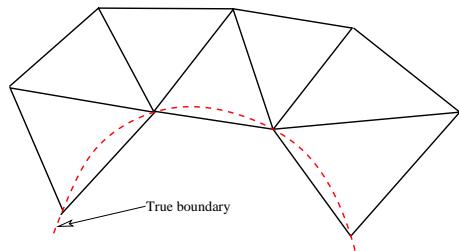


FIG. 8. Mach isolines around a circle with P1Q1 elements on the 128 × 32 grid.
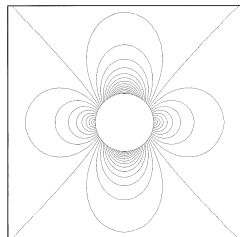


FIG. 12. Mach isolines around a circle with P1Q2 elements on the 128 × 32 grid.

(Bassi & Rebay [6])

# High order meshes

Start with Q1 mesh
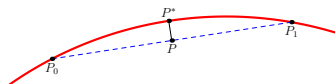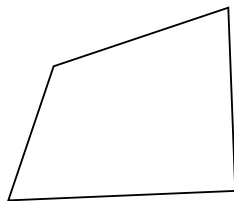


Normal projection of straight
edge onto curved boundary
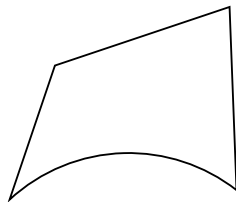
Only boundary edges are high order

# NACA0012 airfoil, M=0.5, AOA=0 deg.

N=3, 1444 cells
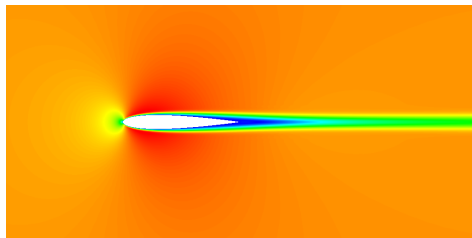


Re=5000

Re=10000
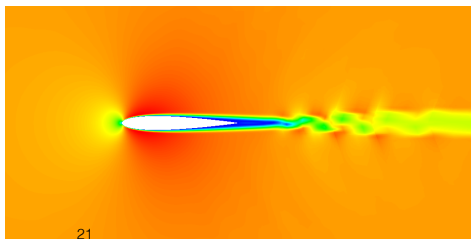
Wake instability due to compressibility effects [8]

# High order meshes
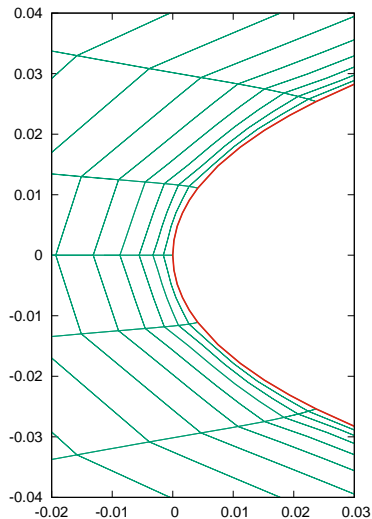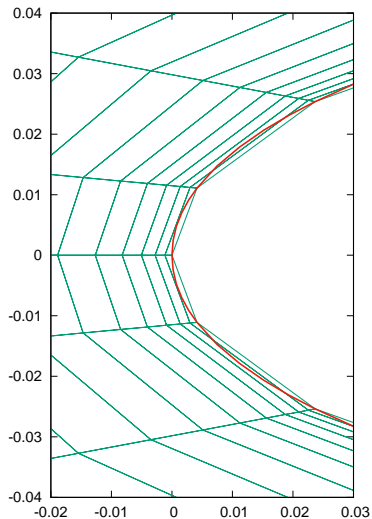


Linear mesh smoothed using Winslow equations

# Winslow-based mapping[2]
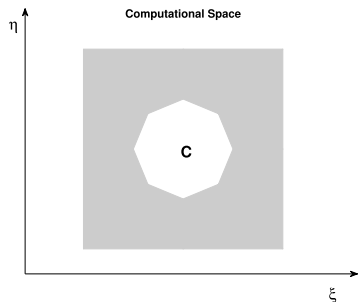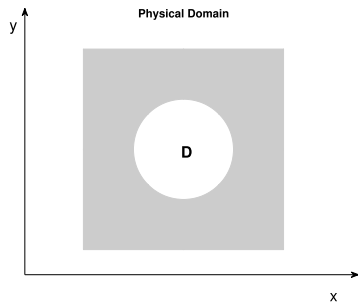


$$g^{ij}\partial_i\partial_j x_k = 0 \quad \text{for } k = 1, \ldots, n,$$

$$g^{ij}g_{jk} = \delta_{ik} \text{ and } g_{ij} = \partial_i x_k \partial_j x_k$$

$$\partial_i(g^{ij}) + \alpha_j = 0, \qquad \text{for } j = 1, \ldots, n,$$

$$\partial_i(g^{ij}\partial_j x_k) + \alpha_j \partial_j x_k = 0, \qquad \text{for } k = 1, \ldots, n.$$

[2]Persson and Fortunato [27]

# Inviscid flow over cylinder
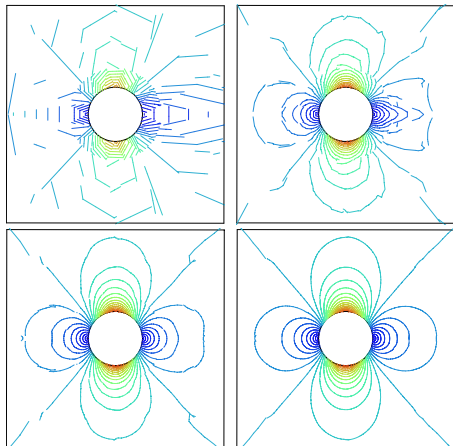


$16 \times 4$ mesh, degrees $1, 2, 3, 4$ (Krivodonova & Berger [37])

# Inviscid flow over cylinder



$h$ vs $p$ refinement
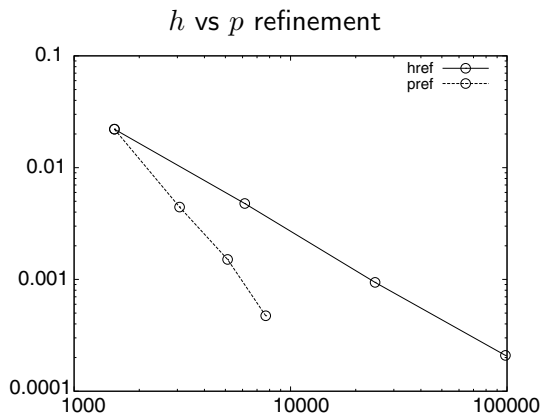
$L_2$ error of total pressure on cylinder surface as function of number of degrees of freedom (Krivodonova & Berger [37])

# Inviscid flow over ellipse
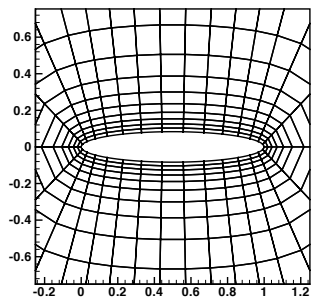


Figure 8.   Closeup of Mesh 1 for the ellipse problem.
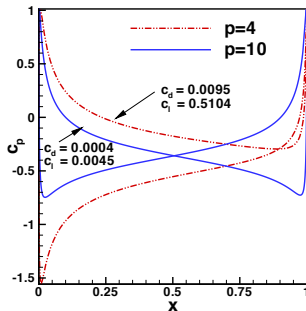


Figure 9.   Pressure coefficient distribution for both Mesh 1 ($p = 4$) and Mesh 2 ($p = 10$).

(Collis & Ghayour, 2003)

# Laminar boundary layer
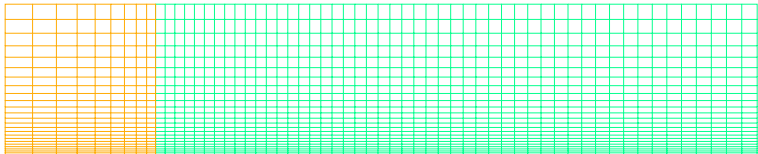


1392 cells, Re=1.5e5, Mach=0.1
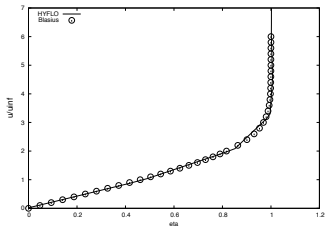


N=1
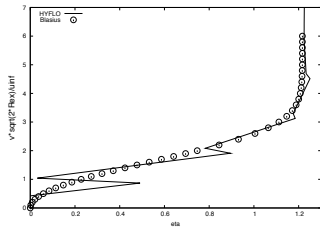
HYFLO

# Laminar boundary layer
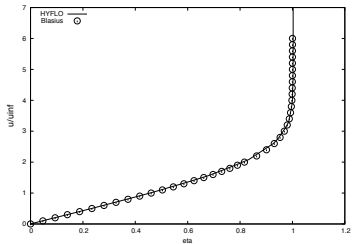


N=2
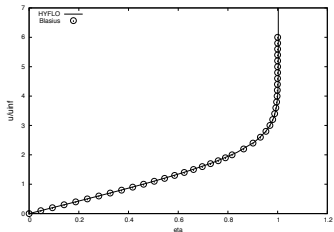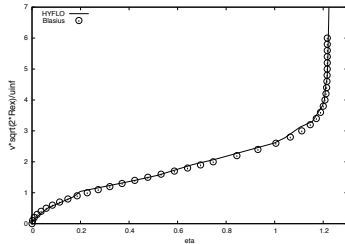
N=3
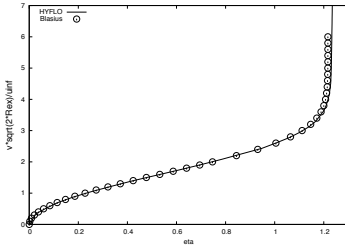
HYFLO

# Boundary conditions

- Imposed weakly through the fluxes
- No-slip bc also imposed weakly
  Gives better accuracy and stability [20]
- Farfield bc can be challenging
  - ▶ wake going upto the boundary
  - ▶ Non-reflecting bc much harder to device
  - ▶ Sponge layers can be used [28], [7], [21], [26]
- Example movie: flow past cylinder

## Entropy variable based schemes

Convex entropy function: $S(\boldsymbol{U}) = -\frac{\rho s}{\gamma - 1}$, $s = \ln(p/\rho^\gamma)$

Entropy variables: $\boldsymbol{V} = \frac{\partial S}{\partial \boldsymbol{U}}$

Used long ago by Deshpande et al. (q-KFVS [32], q-LSKUM [22])

NS in entropy variables

$$\underbrace{\frac{\partial \boldsymbol{U}}{\partial \boldsymbol{V}}}_{spd} \frac{\partial \boldsymbol{V}}{\partial t} + \underbrace{\frac{\partial \boldsymbol{F}_\alpha}{\partial \boldsymbol{V}}}_{sym} \frac{\partial \boldsymbol{V}}{\partial x_\alpha} = \frac{\partial}{\partial x_\alpha} \left( D_{\alpha\beta} \frac{\partial \boldsymbol{V}}{\partial x_\beta} \right)$$

$$D = [D_{\alpha\beta}] = D^\top \geq 0$$

Take dot product with $\boldsymbol{V}$ to get entropy inequality

$$\frac{\partial S}{\partial t} + \nabla \cdot (\boldsymbol{v} S) = \frac{\partial}{\partial x_\alpha} \left( \boldsymbol{V}^\top D_{\alpha\beta} \frac{\partial \boldsymbol{V}}{\partial x_\beta} \right) - \underbrace{\left( \frac{\partial \boldsymbol{V}}{\partial x_\alpha} \right)^\top D_{\alpha\beta} \frac{\partial \boldsymbol{V}}{\partial x_\beta}}_{\geq 0}$$

This property can be mimicked in a DG scheme.

# Entropy variable based schemes

Two ingredients are necessary.

- Need entropy conservative fluxes
  - ▶ Euler equations: Ismail/Roe [36], Chandrashekar [11]
  - ▶ Ideal MHD: Chandrashekar/Klingenberg [12], Winters et al. [46]
- Need exact quadrature to do integration-by-parts
  - ▶ Summation-by-parts property [31], [30]

$\implies$ Semi-discrete entropy stability for any order of accuracy !!!

Beneficial for under-resolved LES and DNS computations [29], [47]

Kinetic energy and/or entropy conserving schemes
$\implies$ behave like central schemes
$\implies$ add explicit SGS model or filtering

For some details, see my lecture slides

## Turbulent flows: DG + RANS

- $k - \omega$ model: [4], [39]
- SA model: [24], [39]
- Very high order may not give much improvement
  $\implies$ limitations of RANS model may play bigger role
- Goal-based grid adaptation
  - ▶ Finite element facilitates adjoint approach

# Turbulent flows: uDNS/ILES

- Inherent dissipation in Riemann solvers acts as implicit SGS model
- Notable successes in computing turbulent and transitional flows
- Instability at very high orders [47]
  $\implies$ inherent dissipation may not be enough
  $\implies$ integration/aliasing errors
- Kinetic energy/entropy preserving schemes, with SBP property may help
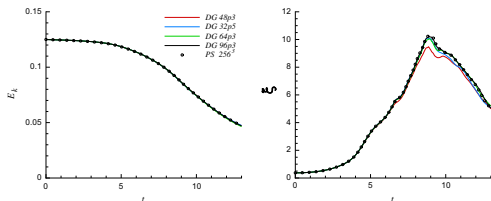


**Fig. 10.** Temporal evolution of mean energy and enstrophy for the TGV computations at $Re = 1600$.
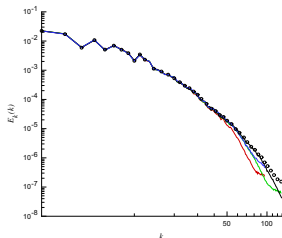


**Fig. 11.** Energy spectra at $t = 8.2$ for the TGV computations at $Re = 1600$. Same legend as Fig. 11.

(Chapelier et al. [13])

# DG for ideal MHD (Guillet et al. [33])
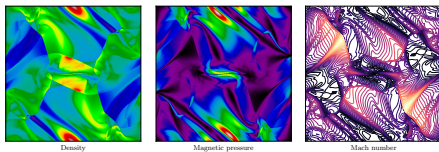


**Figure 10.** *Orszag–Tang vortex test problem at t = 0.5.* The density, pressure and Mach number are shown on a $512^2$ grid, computed using the third-order DG scheme with the Powell method.
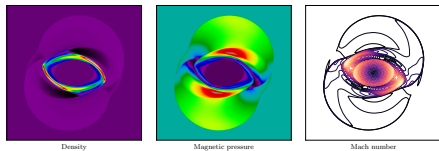


**Figure 16.** *Magnetic rotor test problem.* The density, pressure and Mach number contours in the 2D magnetic adiabatic rotor test are shown, on a $512^2$ grid using the third-order Powell scheme.
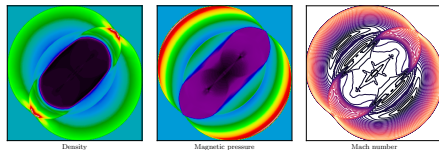


**Figure 20.** *Two-dimensional MHD blast test problem.* The density, magnetic pressure and Mach number contours are shown on a $256^2$ grid using the third-order Powell scheme.

# DG for Maxwell equations (Hazra et al. [35])



IC
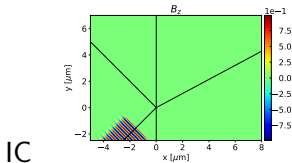
$k = 3$
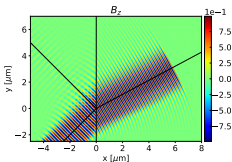
$k = 4$
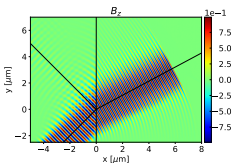
Refraction of compact electromagnetic beam by dielectric slab, $650 \times 475$ cells

IC
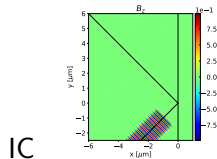
$k = 3$
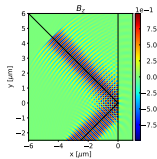
$k = 4$
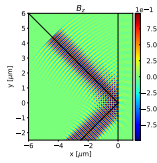
Total internal reflection of compact electromagnetic beam by dielectric slab, $350 \times 425$ cells

# Summary: Advantages

- Very high orders, spectral accuracy
- Low dissipation/dispersion errors
- Good candidate for computing
  - multi-scale phenomena, turbulent flows
  - vortex dominated flows
  - aero-acoustics
- Error independent of time upto $t = O(1/h)$
  useful for long time simulations
- DG is ideal for unstructured grids, hybrid elements
- Local grid refinement: h and p refinement
- Grids with hanging nodes, quadtree/octree grids

# Summary: Issues

- High order meshes essential
- Effect of quadrature on stability
- Effect of inviscid numerical flux [42]
  - $\implies$ both under/over diffusion is harmful
  - $\implies$ Roe-type schemes to be preferred
  - $\implies$ upwind schemes may add too much diffusion at low mach
- Good artificial boundary conditions
- Efficient implementation
  matrix-free, sum factorizations [38]
- Transonic/supersonic turbulence
  - ▶ shock dominated
  - ▶ need limiters or artificial diffusion: effect on accuracy ?

# References

[1] M. ALHAWWARY AND Z. WANG, *Fourier analysis and evaluation of DG, FD and compact difference methods for conservation laws*, Journal of Computational Physics, 373 (2018), pp. 835–862.

[2] D. N. ARNOLD, *An Interior Penalty Finite Element Method with Discontinuous Elements*, SIAM Journal on Numerical Analysis, 19 (1982), pp. 742–760.

[3] D. N. ARNOLD, F. BREZZI, B. COCKBURN, AND L. D. MARINI, *Unified Analysis of Discontinuous Galerkin Methods for Elliptic Problems*, SIAM Journal on Numerical Analysis, 39 (2002), pp. 1749–1779.

[4] F. BASSI, A. CRIVELLINI, S. REBAY, AND M. SAVINI, *Discontinuous Galerkin solution of the Reynolds-averaged Navier–Stokes and k–ω turbulence model equations*, Computers & Fluids, 34 (2005), pp. 507–540.

[5] F. BASSI AND S. REBAY, *A High-Order Accurate Discontinuous Finite Element Method for the Numerical Solution of the Compressible Navier–Stokes Equations*, Journal of Computational Physics, 131 (1997), pp. 267–279.

[6] ———, *High-Order Accurate Discontinuous Finite Element Solution of the 2D Euler Equations*, Journal of Computational Physics, 138 (1997), pp. 251–285.

[7] D. J. BODONY, *Analysis of sponge zones for computational fluid mechanics*, Journal of Computational Physics, 212 (2006), pp. 681–702.

[8] A. BOUHADJI AND M. BRAZA, *Organised modes and shock–vortex interaction in unsteady viscous transonic flows around an aerofoil*, Computers & Fluids, 32 (2003), pp. 1233–1260.

[9] F. BREZZI, G. MANZINI, D. MARINI, P. PIETRA, AND A. RUSSO, *Discontinuous Galerkin approximations for elliptic problems*, Numerical Methods for Partial Differential Equations, 16 (2000), pp. 365–378.

[10] P. CHANDRASHEKAR, *Discontinuous Galerkin method for Navier–Stokes equations using kinetic flux vector splitting*, Journal of Computational Physics, 233 (2013), pp. 527–551.

[11] ———, *Kinetic Energy Preserving and Entropy Stable Finite Volume Schemes for Compressible Euler and Navier-Stokes Equations*, Communications in Computational Physics, 14 (2013), pp. 1252–1286.

# References

[12] P. Chandrashekar and C. Klingenberg, *Entropy Stable Finite Volume Scheme for Ideal Compressible MHD on 2-D Cartesian Meshes*, SIAM Journal on Numerical Analysis, 54 (2016), pp. 1313–1340.

[13] J.-B. Chapelier, M. de la Llave Plata, F. Renac, and E. Lamballais, *Evaluation of a high-order discontinuous Galerkin method for the DNS of turbulent flows*, Computers & Fluids, 95 (2014), pp. 210–226.

[14] Z. Cheng, J. Fang, C.-W. Shu, and M. Zhang, *Assessment of aeroacoustic resolution properties of DG schemes and comparison with DRP schemes*, Journal of Computational Physics, 399 (2019), p. 108960.

[15] B. Cockburn, S. Hou, and C.-W. Shu, *The Runge-Kutta Local Projection Discontinuous Galerkin Finite Element Method for Conservation Laws. IV: The Multidimensional Case*, Mathematics of Computation, 54 (1990), p. 545.

[16] B. Cockburn, S.-Y. Lin, and C.-W. Shu, *TVB Runge-Kutta local projection discontinuous Galerkin finite element method for conservation laws III: One-dimensional systems*, Journal of Computational Physics, 84 (1989), pp. 90–113.

[17] B. Cockburn and C.-W. Shu, *TVB Runge-Kutta local projection discontinuous Galerkin finite element method for conservation laws. II. General framework*, Mathematics of Computation, 52 (1989), pp. 411–411.

[18] ———, *The Local Discontinuous Galerkin Method for Time-Dependent Convection-Diffusion Systems*, SIAM Journal on Numerical Analysis, 35 (1998), pp. 2440–2463.

[19] ———, *The Runge–Kutta Discontinuous Galerkin Method for Conservation Laws V*, Journal of Computational Physics, 141 (1998), pp. 199–224.

[20] S. S. Collis, *Discontinuous Galerkin methods for turbulence simulation*, in Center for Turbulence Research Summer Program, 2002, pp. 155–167.

[21] A. Colombo and A. Crivellini, *Assessment of a sponge layer non-reflecting boundary treatment for high-order CAA/CFD computations*, Computers & Fluids, 140 (2016), pp. 478–499.

[22] S. M. Deshpande, K. Anandhanarayanan, C. Praveen, and V. Ramesh, *Theory and application of 3-D LSKUM based on entropy variables*, International Journal for Numerical Methods in Fluids, 40 (2002), pp. 47–62.

# References

[23] J. Douglas and T. Dupont, *Interior Penalty Procedures for Elliptic and Parabolic Galerkin Methods*, in Computing Methods in Applied Sciences, R. Glowinski and J. L. Lions, eds., vol. 58, Springer Berlin Heidelberg, Berlin, Heidelberg, 1976, pp. 207–216.

[24] M. Drosson and K. Hillewaert, *On the stability of the symmetric interior penalty method for the Spalart–Allmaras turbulence model*, Journal of Computational and Applied Mathematics, 246 (2013), pp. 122–135.

[25] P. Fernandez, R. C. Moura, G. Mengaldo, and J. Peraire, *Non-modal analysis of spectral element methods: Towards accurate and robust large-eddy simulations*, Computer Methods in Applied Mechanics and Engineering, 346 (2019), pp. 43–62.

[26] D. Flad, A. D. Beck, G. Gassner, and C.-D. Munz, *A Discontinuous Galerkin Spectral Element Method for the direct numerical simulation of aeroacoustics*, in 20th AIAA/CEAS Aeroacoustics Conference, Atlanta, GA, June 2014, American Institute of Aeronautics and Astronautics.

[27] M. Fortunato and P.-O. Persson, *High-order unstructured curved mesh generation using the Winslow equations*, Journal of Computational Physics, 307 (2016), pp. 1–14.

[28] J. B. Freund, *Proposed Inflow/Outflow Boundary Condition for Direct Computation of Aerodynamic Sound*, AIAA Journal, 35 (1997), pp. 740–742.

[29] G. J. Gassner, *A kinetic energy preserving nodal discontinuous Galerkin spectral element method: KEP-DGSEM*, International Journal for Numerical Methods in Fluids, 76 (2014), pp. 28–50.

[30] G. J. Gassner, A. R. Winters, F. J. Hindenlang, and D. A. Kopriva, *The BR1 Scheme is Stable for the Compressible Navier–Stokes Equations*, Journal of Scientific Computing, 77 (2018), pp. 154–200.

[31] G. J. Gassner, A. R. Winters, and D. A. Kopriva, *Split form nodal discontinuous Galerkin schemes with summation-by-parts property for the compressible Euler equations*, Journal of Computational Physics, 327 (2016), pp. 39–66.

# References

[32]  A. K. Ghosh, J. S. Mathur, and S. M. Deshpande, *Q-KFVS scheme — A new higher order kinetic method for euler equations*, in Sixteenth International Conference on Numerical Methods in Fluid Dynamics, C.-H. Bruneau, ed., vol. 515, Springer Berlin Heidelberg, 1998, pp. 379–384.

[33]  T. Guillet, R. Pakmor, V. Springel, P. Chandrashekar, and C. Klingenberg, *High-order magnetohydrodynamics for astrophysics with an adaptive mesh refinement discontinuous Galerkin scheme*, Monthly Notices of the Royal Astronomical Society, 485 (2019), pp. 4209–4246.

[34]  R. Hartmann and P. Houston, *An optimal order interior penalty discontinuous Galerkin discretization of the compressible Navier–Stokes equations*, Journal of Computational Physics, 227 (2008), pp. 9670–9685.

[35]  A. Hazra, P. Chandrashekar, and D. S. Balsara, *Globally constraint-preserving FR/DG scheme for Maxwell's equations at all orders*, Journal of Computational Physics, 394 (2019), pp. 298–328.

[36]  F. Ismail and P. L. Roe, *Affordable, entropy-consistent Euler flux functions II: Entropy production at shocks*, Journal of Computational Physics, 228 (2009), pp. 5410–5436.

[37]  L. Krivodonova and M. Berger, *High-order accurate implementation of solid wall boundary conditions in curved geometries*, Journal of Computational Physics, 211 (2006), pp. 492–512.

[38]  M. Kronbichler and K. Kormann, *A generic interface for parallel cell-based finite element operator application*, Computers & Fluids, 63 (2012), pp. 135–147.

[39]  B. Landmann, *A parallel discontinuous Galerkin code for the Navier-Stokes and Reynolds-averaged Navier-Stokes equations*, June 2008.

[40]  H. Luo, J. D. Baum, and R. Löhner, *A discontinuous Galerkin method based on a Taylor basis for the compressible flows on arbitrary grids*, Journal of Computational Physics, 227 (2008), pp. 8875–8893.

[41]  G. Mengaldo, R. Moura, B. Giralda, J. Peiró, and S. Sherwin, *Spatial eigensolution analysis of discontinuous Galerkin schemes with practical insights for under-resolved computations and implicit LES*, Computers & Fluids, 169 (2018), pp. 349–364.

# References

[42]  R. Moura, S. Sherwin, and J. Peiró, *Linear dispersion–diffusion analysis and its application to under-resolved turbulence simulations using discontinuous Galerkin spectral/ hp methods*, Journal of Computational Physics, 298 (2015), pp. 695–710.

[43]  J. Peraire and P.-O. Persson, *The Compact Discontinuous Galerkin (CDG) Method for Elliptic Problems*, SIAM Journal on Scientific Computing, 30 (2008), pp. 1806–1824.

[44]  K. Schaal, A. Bauer, P. Chandrashekar, R. Pakmor, C. Klingenberg, and V. Springel, *Astrophysical hydrodynamics with a high-order discontinuous Galerkin scheme and adaptive mesh refinement*, Monthly Notices of the Royal Astronomical Society, 453 (2015), pp. 4278–4300.

[45]  C.-W. Shu and S. Osher, *Efficient Implementation of Essentially Non-oscillatory Shock-capturing Schemes*, J. Comput. Phys., 77 (1988), pp. 439–471.

[46]  A. R. Winters and G. J. Gassner, *Affordable, entropy conserving and entropy stable flux functions for the ideal MHD equations*, Journal of Computational Physics, 304 (2016), pp. 72–108.

[47]  A. R. Winters, R. C. Moura, G. Mengaldo, G. J. Gassner, S. Walch, J. Peiro, and S. J. Sherwin, *A comparative study on polynomial dealiasing and split form discontinuous Galerkin schemes for under-resolved turbulence computations*, Journal of Computational Physics, 372 (2018), pp. 1–21.

[48]  M. Zhang and C.-W. Shu, *AN ANALYSIS OF THREE DIFFERENT FORMULATIONS OF THE DISCONTINUOUS GALERKIN METHOD FOR DIFFUSION EQUATIONS*, Mathematical Models and Methods in Applied Sciences, 13 (2003), pp. 395–413.

# Thank You